

# Bounds on the renormalized couplings in an $SU(2)_L \otimes SU(2)_R$ symmetric Yukawa model

L. Lin\*    I. Montvay†    G. Münster\*    M. Plagge\*    H. Wittig‡

March 23, 1993

## Abstract

The vacuum stability lower bound on the mass of the Higgs boson is numerically investigated in an  $SU(2)_L \otimes SU(2)_R$  symmetric Yukawa model, which describes two heavy degenerate fermion doublets in the limit of vanishing gauge couplings. Good agreement with perturbation theory is found, although the couplings are strong. The upper bound on the fermion mass and renormalized Yukawa coupling is also determined in the part of bare parameter space where reflection positivity has been proven.

## 1 Introduction

Cut-off dependent upper bounds on renormalized couplings arise in the Standard Model for non-asymptotically free couplings, if their continuum limit is trivial. Such “triviality bounds” show up in perturbation theory as an apparent inconsistency [1], and have been intensively studied on the lattice by non-perturbative methods (for a recent review see [2]). In Yukawa models there is also a lower limit on the Higgs mass, which is called “vacuum stability bound” [3]. On the lattice this can be understood as due to quantum effects inducing a positive renormalized quartic scalar coupling even if the bare quartic coupling takes its lowest possible value, namely zero [4].

In previous papers [5] the triviality upper bound on the Higgs mass has been investigated by non-perturbative methods in a Yukawa model with chiral  $SU(2)_L \otimes SU(2)_R$  symmetry. The lattice formulation is based on the mirror fermion action [6] with exact decoupling of the mirror fermions from the physical spectrum [7, 8]. (Another lattice formulation of the same continuum “target theory” is possible by using reduced staggered fermions [9].) Since the Hybrid Monte Carlo method [10] is used, the minimum number of fermion doublets which can be numerically simulated, is two. In this context it is important that we are working in the limit of vanishing

---

\*Institut für Theoretische Physik I, Universität Münster, Wilhelm-Klemm-Str. 9, D-4400 Münster, FRG

†Deutsches Elektronen-Synchrotron DESY, Notkestr. 85, D-2000 Hamburg 52, FRG

‡Department of Theoretical Physics, University of Southampton, UK

gauge couplings, and hence by charge conjugation a mirror fermion doublet can be transformed to a fermion doublet. In fact, only the vanishing of the  $SU(3)_{\text{colour}} \otimes U(1)_{\text{hypercharge}}$  gauge couplings is necessary. The chiral  $SU(2)_L$  gauge coupling can be introduced, because  $SU(2)$  is pseudoreal [11, 12].

In the present paper we continue the non-perturbative investigation of the same  $SU(2)_L \otimes SU(2)_R$  symmetric Yukawa model as in refs. [13, 5]. In particular, we concentrate on the vacuum stability lower bound and on the upper limit of the renormalized Yukawa coupling in the region of positive scalar hopping parameter, where reflection positivity, implying unitarity in Minkowski space, can be proven [4]. Besides the physically relevant phase with broken symmetry, the renormalized Yukawa coupling is also computed in the symmetric phase, in order to check previous observations of very strong couplings there [14, 13].

## 2 Vacuum stability bound

The lattice action and the definition of different renormalized physical quantities closely follow our previous papers on chiral Yukawa models with mirror fermions [14, 4, 13, 5]. The lattice action is a sum of the  $O(4)$  ( $\cong SU(2)_L \otimes SU(2)_R$ ) symmetric pure scalar part  $S_\varphi$  and fermionic part  $S_\Psi$ :

$$S = S_\varphi + S_\Psi. \quad (1)$$

$\varphi_x$  is the  $2 \otimes 2$  matrix scalar field, and  $\Psi_x \equiv (\psi_x, \chi_x)$  stands for the mirror pair of fermion doublet fields (usually  $\psi$  is the fermion doublet and  $\chi$  the mirror fermion doublet). In the usual normalization conventions for numerical simulations we have

$$\begin{aligned} S_\varphi &= \sum_x \left\{ \frac{1}{2} \text{Tr}(\varphi_x^+ \varphi_x) + \lambda \left[ \frac{1}{2} \text{Tr}(\varphi_x^+ \varphi_x) - 1 \right]^2 - \kappa \sum_{\mu=1}^4 \text{Tr}(\varphi_{x+\hat{\mu}}^+ \varphi_x) \right\}, \\ S_\Psi &= \sum_x \left\{ \mu_{\psi\chi} \left[ (\bar{\chi}_x \psi_x) + (\bar{\psi}_x \chi_x) \right] \right. \\ &\quad \left. - K \sum_{\mu=\pm 1}^{\pm 4} \left[ (\bar{\psi}_{x+\hat{\mu}} \gamma_\mu \psi_x) + (\bar{\chi}_{x+\hat{\mu}} \gamma_\mu \chi_x) + r \left( (\bar{\chi}_{x+\hat{\mu}} \psi_x) - (\bar{\chi}_x \psi_x) + (\bar{\psi}_{x+\hat{\mu}} \chi_x) - (\bar{\psi}_x \chi_x) \right) \right] \right. \\ &\quad \left. + G_\psi \left[ (\bar{\psi}_{Rx} \varphi_x^+ \psi_{Lx}) + (\bar{\psi}_{Lx} \varphi_x \psi_{Rx}) \right] + G_\chi \left[ (\bar{\chi}_{Rx} \varphi_x \chi_{Lx}) + (\bar{\chi}_{Lx} \varphi_x^+ \chi_{Rx}) \right] \right\}. \end{aligned} \quad (2)$$

Here  $K$  is the fermion hopping parameter,  $r$  the Wilson-parameter, which will be fixed to  $r = 1$  in the numerical simulations, and the indices  $L, R$  denote, as usual, the chiral components of fermion fields. In this normalization the fermion–mirror-fermion mixing mass is  $\mu_{\psi\chi} = 1 - 8rK$ .

The fermionic part  $S_\Psi$  is given here for a single mirror pair of fermions. For the Hybrid Monte Carlo simulation the fermions have to be doubled by taking the adjoint of the fermion matrix for the new species. Taking the adjoint transforms fermions to mirror fermions and vice versa, but as noted before, without  $SU(3)_{\text{colour}} \otimes U(1)_{\text{hypercharge}}$  gauge couplings they are equivalent to each other.

The numerical simulations were performed on  $6^3 \cdot 12$  lattices at a bare scalar quartic coupling  $\lambda = 10^{-6}$ . The small positive value of  $\lambda$  was chosen in order to be sure about the convergence of the path integral. The Yukawa coupling  $G_\chi$  was kept at zero, for exact decoupling of the mirror doublets [8]. This allows to stay with the fermion hopping parameter  $K$  near its critical value at  $K = 1/8$ , as described in ref. [5]. In the broken (FM) phase at the fixed values  $G_\psi = 0.25$  and  $G_\chi = 0.30$  the scalar hopping parameter was tuned to achieve a scalar mass of about

Table 1: The main renormalized quantities and the bare magnetization  $\langle\sigma\rangle \equiv \langle|\varphi|\rangle$  for several bare couplings  $G_\psi$  and  $\kappa$ -values. Points labelled by small letters are our data at  $\lambda = 10^{-6}$  which were all obtained on  $6^3 \cdot 12$ . Points labelled by capital letters are the data for the upper bound at  $\lambda = \infty$ . For the points with double capital letters the lattice size was  $8^3 \cdot 16$ , whereas single capital letters denote data on  $6^3 \cdot 12$ . All data are collected from typically 10000 trajectories, except for the points labelled a, i, A, C where only about 5000 trajectories were run. As  $G_\chi = 0$ , the renormalized coupling  $G_{R\chi}$  was always zero within errors and is not included here.

	$G_\psi$	$\kappa$	$\langle\sigma\rangle$	$v_R$	$m_{R\sigma}$	$\mu_{R\psi}$	$g_R$	$G_{R\psi}$	$G_{R\psi}^{(3)}$
a	0.25	0.095	0.251(7)	0.196(11)	0.79(7)	0.271(8)	42(11)	1.38(4)	1.42(20)
b	0.25	0.099	0.393(7)	0.241(10)	0.59(9)	0.407(9)	18(3)	1.69(4)	1.56(16)
c	0.25	0.101	0.525(6)	0.304(9)	0.57(3)	0.59(3)	10(2)	1.68(10)	1.53(40)
d	0.3	0.090	0.438(6)	0.27(1)	0.75(7)	0.55(6)	23(3)	2.04(10)	
e	0.3	0.095	0.754(4)	0.417(11)	0.76(7)	0.91(6)	10(1)	2.19(11)	
f	0.3	0.100	1.260(5)	0.67(2)	0.84(6)	1.503(12)	4.8(8)	2.24(7)	
g	0.62	0.0	0.424(3)	0.29(2)	1.23(9)	1.23(3)	53(11)	4.2(1.2)	4.5(4.0)
h	0.63	0.0	0.469(3)	0.351(11)	1.65(13)	1.25(16)	63(16)	3.5(4)	
i	0.65	0.0	0.523(3)	0.34(2)	1.39(14)	1.6(3)	53(18)	4.6(4)	
A	0.3	0.30	0.439(1)	0.400(13)	1.17(7)	0.55(2)	26(7)	1.36(6)	
BB	0.3	0.27	0.270(2)	0.25(1)	0.77(3)	0.342(2)	31(4)	1.35(6)	1.36(12)
C	0.6	0.18	0.3524(18)	0.36(2)	1.36(10)	0.86(8)	36(6)	2.4(3)	
DD	0.6	0.18	0.3389(13)	0.339(16)	1.31(7)	0.86(11)	38(4)	2.5(3)	2.3(2.4)

$m_{R\sigma} \simeq 0.6 - 0.8$  and a not too small fermion mass.  $\kappa$  was always kept to be non-negative, in order to be sure about reflection positivity, that is unitarity in Minkowski space [4]. The last points in the positivity region were fixed at  $\kappa = 0$ , and then  $G_\psi$  was tuned to obtain reasonable masses. The results are summarized in table 1, where also such points are included where the masses are not yet sufficiently tuned.

Tuning the scalar and fermion mass is, of course, important in order to be close to the critical line separating the broken (FM) and symmetric (PM) phases [15], and at the same time avoid strong finite size effect. This prevents us from going on the  $6^3 \cdot 12$  lattice to a very small Yukawa coupling  $G_\psi \ll 1$ , because then the fermion mass becomes too small. At the strongest Yukawa coupling (at  $\kappa = 0$ ) the minimum of the scalar mass on our lattice is quite large (above 1), therefore we could not achieve the desired value  $m_{R\sigma} \simeq 0.6 - 0.8$ . This is similar to the behaviour observed at  $\lambda = \infty$  [5]. More generally, in the investigated range of  $G_\psi$  the qualitative change of the renormalized quantities between  $4^3 \cdot 8$  and  $6^3 \cdot 12$  lattices is quite similar to the one at  $\lambda = \infty$ . This allows to choose the points with label c,d and g as optimal in the three sets of points for the lower bound in table 1. These are shown in figs. 1 and 2 together with the one-loop perturbative estimates of the vacuum stability lower limit at the given cut-offs. In these figures also the data at  $\lambda = \infty$  are included, which show the behaviour of the triviality upper bound for the renormalized quartic coupling. For completeness we display the results for  $\lambda = \infty$  in table 1 too, because more statistics has been collected for some points since publication of [5].

The agreement between numerical simulation data and the one-loop perturbative estimates

is remarkably good. In particular, at the strongest couplings, within our errors, there is practically no difference in the renormalized couplings between  $\lambda \simeq 0$  and  $\lambda = \infty$ . This means that the strong Yukawa coupling alone is able to induce the maximal possible renormalized quartic coupling at the given cut-off.

Table 1 also includes results for the renormalized Yukawa coupling  $G_{R\psi}^{(3)}$ , defined in terms of a three-point function (see [5]). At tree level, and moreover in the one-loop approximation, it coincides with  $G_{R\psi}$ . The numerical results show that both couplings are consistent with each other, even in those points where the errors are relatively large.

### 3 Yukawa coupling

One can see in table 1 that in the broken (FM) phase the renormalized Yukawa coupling  $G_{R\psi}$  grows with the bare coupling  $G_\psi$  roughly linearly, up to quite strong values above the tree unitarity limit  $\sqrt{2\pi} \simeq 2.5$ . In previous numerical simulations in the symmetric (PM) phase of the  $U(1)_L \otimes U(1)_R$  [14] and  $SU(2)_L \otimes SU(2)_R$  [13] symmetric Yukawa models very strong renormalized Yukawa couplings were observed, as well. We would like to see how strong the renormalized Yukawa couplings can be in the PM phase in the mirror-fermion decoupling limit. Since we do not want to go to the region with  $\kappa < 0$  where reflection positivity could not be proven [4], the maximal possible value of  $G_{R\psi}$  should come from tuning  $G_\psi$  along the  $\kappa = 0$  axis in the PM phase. We tune  $G_\psi$  such that the physical scalar mass  $m_\phi$  is around 0.7 on the  $6^3 \cdot 12$  lattice to avoid large finite size effects. We also run the same point on  $8^3 \cdot 12$  and  $8^3 \cdot 16$  lattices to see how various quantities (especially the renormalized Yukawa couplings) change with different volumes.

The renormalized Yukawa coupling matrix  $G_R \equiv \text{diag}(G_{R\psi}, G_{R\chi})$  is defined as

$$G_R \equiv -\frac{m_R^2}{4\sqrt{Z_R}} \tilde{\Gamma}_R(k) Z_\Psi^{-1/2} \langle \Phi \Psi \bar{\Psi} \rangle_0 Z_\Psi^{-1/2} \tilde{\Gamma}_R(k), \quad (3)$$

where the three-point Green's function  $\langle \Phi \Psi \bar{\Psi} \rangle_0$  and  $Z_\Psi^{-1/2}$  are defined in [13].  $\tilde{\Gamma}_R(k)$  is the momentum-space renormalized fermionic two-point vertex function defined at the smallest momentum  $k = (\vec{0}, k_4)$ ,  $k_4 = \pi/T$ . Near  $k = 0$  the behaviour of  $\tilde{\Gamma}_R(k)$  is

$$\tilde{\Gamma}_R(k) \simeq i\gamma_4 \bar{k}_4 + M_R, \quad \bar{k}_4 \equiv \text{sink}_4 = \sin\left(\frac{\pi}{T}\right), \quad M_R = \begin{pmatrix} 0 & \mu_R \\ \mu_R & 0 \end{pmatrix}, \quad (4)$$

where  $\mu_R$  is the renormalized fermion mass. In previous work we did the leading-order approximation by neglecting the term  $i\gamma_4 \bar{k}_4$  in the measurement since  $T$  is large. However, from data in [13], we suspect that it might cause some small but visible effects on  $G_R$ . Therefore we decided to improve the measurement of  $G_R$  by including this leading-order correction. Also, we remove a previous inconsistency in normalization in the definition of  $G_R$  in the PM phase. Before, the convention was such that the full scalar propagator at zero momentum  $\tilde{G}(0) \equiv \sum_{x,y} \langle \phi_{Sx} \phi_{Sy} \rangle / L^3 T$ , after renormalization, was normalized to  $1/m_R^2$ . However, this does not correspond to the natural normalization convention we used in the broken phase [5]. There the convention corresponds to the one in the PM phase such that  $\tilde{G}(0)$  is renormalized to  $4/m_R^2$ . In order to have a fair comparison of the renormalized Yukawa couplings in both phases, we decide to switch to this new convention of normalization for  $G_R$  shown in (3). This implies that data on  $G_R$ 's in [13] should be scaled down by a factor of two in this new normalization

convention. (A similar inconsistency in the  $U(1)_L \otimes U(1)_R$  symmetric model [14] can be removed by dividing the values of  $G_R$  there by a factor of  $\sqrt{2}$ .)

One should notice that, as shown in (3), scalar quantities appearing in the definition of  $G_R$  should be the renormalized scalar mass  $m_R$  and the wave function renormalization factor  $Z_R$  defined at vanishing momentum [16]. However, the scalar mass we actually use in the measurement is the physical scalar mass  $m_\phi$  obtained from a  $\cosh$  fit of the scalar field correlation function along the time direction. The wave function renormalization factor  $Z_3$ , which is defined through the residuum of the pole of the propagator, cannot be determined reliably from our statistics. Therefore we define the wave function renormalization factor  $Z_\phi$  in terms of the mass  $m_\phi$  and the susceptibility  $\tilde{G}(0)$  by means of

$$Z_\phi = m_\phi^2 \tilde{G}(0). \quad (5)$$

In general,  $m_R$  and  $Z_R$  is different from  $m_\phi$  and  $Z_\phi$ . In a weakly interacting system (e.g. pure scalar  $\lambda\phi^4$  theory), they are very close to each other [16]. In our  $SU(2)$  mirror-fermion model, the bare Yukawa coupling  $G_\psi$  is large, therefore there is no guarantee that they are still close to each other. On the other hand, the correct measurement of  $m_R$  and  $Z_R$  is crucial to the measurement of  $G_{R\psi}$  and  $G_{R\chi}$ , we therefore also measure  $m_R$  and  $Z_R$  to see how they differ from  $m_\phi$  and  $Z_\phi$ . Since we are on the finite lattice, we estimate  $Z_R$  and  $m_R$  from

$$Z_R^{-1} \equiv [\tilde{G}(k)^{-1} - \tilde{G}(0)^{-1}] / \hat{k}^2, \quad m_R^2 = \frac{Z_R}{\tilde{G}(0)}, \quad (6)$$

where

$$k = (\vec{0}, k_4), \quad k_4 = \frac{2\pi}{T}, \quad \hat{k}^2 = 4\sin^2\left(\frac{k_4}{2}\right). \quad (7)$$

The results of the numerical simulations in the symmetric phase are collected in table 2. From the table one can clearly see that  $G_{R\chi}$  is now zero within error bars as expected from the shift symmetry at  $G_\chi = 0$  [8, 13]. This indicates that the term we used to neglect does, indeed, have some visible effect on the renormalized Yukawa couplings. Meanwhile, the natural definition of the renormalized couplings are taken at zero momentum since there is no infrared singularity in the PM phase. But  $G_R$ 's we measured according to (3) are actually defined at  $k = (0, 0, 0, \pi/T)$ , which will approach zero in the infinite  $T$  limit. If the inverse propagator had a non-negligible curvature near zero momentum, this would influence the determination of  $Z_R$  and hence of other renormalized quantities. We therefore took measurements at two different values of  $T$ , i.e.:  $T = 12, 16$ , to see how we can get  $G_R$ 's at zero momentum by extrapolation. Our data show that  $G_{R\psi}$  and  $G_{R\chi}$  basically stay unchanged as  $T$  goes from 12 to 16. We therefore believe that curvature effects in the propagator are not large and that the data we have on  $G_R$ 's are, to a good approximation, the renormalized Yukawa couplings defined at zero momentum.

The fluctuations of  $Z_R$  and  $m_R$  are quite large, as expected. Within error bars, they agree with  $Z_\phi$  and  $m_\phi$ . This shows that our measurement of  $G_{R\psi}$  and  $G_{R\chi}$  using  $m_\phi$  and  $Z_\phi$  can be taken as a good approximation to the  $G_R$ 's defined in (3).

As one can see from table 2, on our lattices the maximal value of  $G_{R\psi}$  in the region of non-negative scalar hopping parameter is more than twice the value of the tree unitarity bound. This supports our previous results in the symmetric phase on smaller lattices and less statistics [14, 13]. With the present correct normalization the difference between the maximal value of  $G_{R\psi}$  in the symmetric and broken phase is not dramatic, although the values are still larger in the symmetric phase (see tables 1–2).

Table 2: The main renormalized quantities at  $\lambda = \infty$ ,  $G_\chi = 0$ ,  $G_\psi = 1.09$ ,  $\kappa = 0$  and  $K = 2/19$  in the PM phase on various lattices. Data on  $6^3 \cdot 12$  lattices are collected from 20000 trajectories while on  $8^3 \cdot 12$  and  $8^3 \cdot 16$  we have about 6000 trajectories each.

Size	$m_\phi$	$m_R$	$Z_\phi$	$Z_R$	$\mu_R$	$G_{R\psi}$	$G_{R\chi}$
$6^3 \cdot 12$	0.69(3)	0.60(17)	1.52(5)	1.11(38)	0.664(5)	5.84(16)	-0.03(7)
$8^3 \cdot 12$	0.65(7)	0.56(11)	1.84(15)	1.36(57)	0.654(9)	6.04(37)	-0.12(17)
$8^3 \cdot 16$	0.55(3)	0.51(11)	1.71(33)	1.44(73)	0.63(1)	5.87(54)	0.07(9)

## 4 $1/N$ expansion

The results of numerical studies of the phase diagram of the model at both  $\lambda = \infty$  and  $\lambda = 10^{-6}$  are reported in [5]. The particular interest in the phase structure at small  $\lambda$  arose after it was reported [17] that models with naive fermions do not exhibit a ferrimagnetic (FI) phase and that instead a first order phase transition is observed. Clearly the absence of any such transition is of great importance for the study of bounds on the couplings within our model.

Our Monte Carlo investigations show that at least the physically relevant phase transition from the PM to the FM phase is second order. In particular, the magnetization varies smoothly across the transition.

The numerical analysis of the phase diagram was supplemented by a  $1/N_f$  expansion in leading order, where  $N_f$  denotes the number of fermion–mirror-fermion doublet pairs.

Our strategy was to calculate the one-loop effective potential to leading order in  $1/N_f$  as a function of the fluctuation field

$$\sigma_x \equiv \phi_{4x} - s - (-1)^{x_1+x_2+x_3+x_3} \hat{s}, \quad (8)$$

where  $\phi_{4x}$  is the fourth real component of the scalar field  $\varphi_x$ , and  $s$  and  $\hat{s}$  are the positions of the minimum of the effective potential at tree level with respect to  $\varphi_x$  and the staggered scalar field  $\hat{\varphi}_x$ , respectively. After performing a Fourier transformation to momentum space, we finally obtain the effective potential  $V_{\text{eff}}[\tilde{\sigma}(0), \tilde{\sigma}(\pi)]$  as a function of the fluctuation field at both the zero- and  $4\pi$ -corners of the Brillouin zone. The qualitative features of the transitions from PM to FM (PM to AFM [15]) can now be studied via the dependence of  $V_{\text{eff}}$  on the field  $\tilde{\sigma}(0)$  (the field  $\tilde{\sigma}(\pi)$ ).

A first observation is that to leading order in  $1/N_f$  the effective potential is a quadratic function of  $\tilde{\sigma}(0)$  and  $\tilde{\sigma}(\pi)$ , and therefore we do not expect a first order phase transition which would rather require a quartic term, resulting in a double-well structure of the potential.

For  $\lambda = 0$  we obtain estimates for the critical value of the scalar hopping parameter  $\kappa$  from the two gap equations

$$-16\kappa_{\text{cr}} + 2 - 8N_f G_\psi^2 \int_q \frac{\bar{q}^2}{(\bar{q}^2 + \mu_q^2)^2 + G_\psi^2 s^2 \bar{q}^2} = 0 \quad (\text{for PM} \leftrightarrow \text{FM}), \quad (9)$$

$$16\kappa_{\text{cr}} + 2 = 0 \quad (\text{for PM} \leftrightarrow \text{AFM}), \quad (10)$$

where  $\bar{q}_\mu = \sin(q_\mu)$ , and the integral is taken over the Brillouin zone. It is therefore only the transition PM to FM which is affected by fermionic contributions in leading order. Its transition line bends down for increasing Yukawa couplings and finally intersects the straight transition

line from PM to AFM at  $\kappa_{\text{cr}} = -1/8$ . Obviously, in leading order of the  $1/N_f$  expansion the qualitative behaviour of the phase transition lines is similar to all our numerical studies [5, 15].

According to the  $1/N_f$  expansion the FI phase exists in leading order, since solutions to the minimum of  $V_{\text{eff}}$  at non-zero values of both  $\tilde{\sigma}(0)$  and  $\tilde{\sigma}(\pi)$  are found to exist. Furthermore, the position of the minimum of  $V_{\text{eff}}$  varies smoothly across all phase transition lines, therefore suggesting the existence of second order phase transitions only.

The findings from the  $1/N_f$  expansion together with the Monte Carlo results are strong evidence that the allowed region of renormalized couplings can safely be studied at  $\lambda \simeq 0$  as well.

## 5 Conclusions

The main conclusion of the numerical simulations of heavy fermions in the  $SU(2)_L \otimes SU(2)_R$  symmetric Yukawa model is that the estimates of the upper and lower bounds on renormalized couplings obtained in one-loop perturbation theory work well. All qualitative features of the one-loop  $\beta$ -functions are supported, including the fixed point in the ratio of the fermion to scalar mass  $\mu_{R\psi}/m_{R\sigma}$  (see fig. 2). The upper limit of the renormalized couplings (at the fixed ratio of  $g_R/G_{R\psi}^2$ ) is provided by our requirement of reflection positivity. If this would not be imposed, the line towards the upper right corner of fig. 1 would be continued, but probably not much beyond our values. The reason is the appearance of the ferrimagnetic (FI) phase transition in the region of negative scalar hopping parameters, somewhat beyond the maximal bare Yukawa coupling we consider. The existence of the FI phase at small and large values of the bare quartic coupling  $\lambda$  is implied by both numerical simulations and  $1/N$  expansion. These conclusions are also supported in a recent numerical simulation of the same continuum “target theory” as ours, by using reduced staggered fermions [18].

Although the observed qualitative behaviour is certainly consistent with the one-loop perturbative scenario implying the triviality of the continuum limit, one has to keep in mind that present simulations are done at relatively low cut-offs. In particular, the evolution of the couplings towards smaller values at decreasing cut-offs should be investigated in the future. At present the renormalized Yukawa coupling can have quite large values (see tables 1–2). In the symmetric phase it reaches more than twice the tree level unitarity bound with both scalar and fermion masses about equal to 0.5 in lattice units.

## Acknowledgements

We thank Christoph Frick for useful discussions. The Monte Carlo calculations for this work have been performed on the CRAY Y-MP/832 of HLRZ Jülich.

## References

- [1] L.D. Landau, I.Y. Pomeranchuk, Dokl. Akad. Nauk SSSR 102 (1955) 489.
- [2] D.N. Petcher, review talk at the Lattice '92 Conference in Amsterdam, 1992, to be published in Nucl. Phys. B (Proc. Suppl.).
- [3] M.J. Duncan, R. Philippe, M. Sher, Phys. Lett. B153 (1985) 165;  
M. Sher, Phys. Rep. 179 (1989) 273.
- [4] L. Lin, I. Montvay, G. Münster, H. Wittig, Nucl. Phys. B355 (1991) 511.
- [5] C. Frick, L. Lin, I. Montvay, G. Münster, M. Plagge, T. Trappenberg, H. Wittig, DESY Preprint 92-111, to appear in Nucl. Phys. B;  
DESY preprint 92-183, to appear in Nucl. Phys. B (Proc. Suppl.).
- [6] I. Montvay, Phys. Lett. B199 (1987) 89;  
Nucl. Phys. B (Proc. Suppl.) 4 (1988) 443.
- [7] A. Borrelli, L. Maiani, G.C. Rossi, R. Sisto, M. Testa, Phys. Lett. B221 (1989) 360.
- [8] M.F.L. Golterman, D.N. Petcher, Phys. Lett. B225 (1989) 159.
- [9] J. Smit, Nucl. Phys. B (Proc. Suppl.) 26 (1992) 480;  
W. Bock, J. Smit, J.C. Vink, Phys. Lett. B291 (1992) 297;  
Amsterdam preprint, ITFA-92-31 (1992).
- [10] S. Duane, A.D. Kennedy, B.J. Pendleton, D. Roweth, Phys. Lett. B195 (1987) 216.
- [11] I. Montvay, Nucl. Phys. B (Proc. Suppl.) 29B,C (1992) 159.
- [12] I. Montvay, CERN preprint TH. 6717/92 (1992), to appear in Nucl. Phys. B (Proc. Suppl.).
- [13] L. Lin, H. Wittig, Z. Phys. C54 (1992) 331.
- [14] K. Farakos, G. Koutsoumbas, L. Lin, J. P. Ma, I. Montvay, G. Münster, Nucl. Phys. B350 (1991) 474.
- [15] L. Lin, I. Montvay, H. Wittig, Phys. Lett. B264 (1991) 407.
- [16] C. Frick, K. Jansen, J. Jersák, I. Montvay, P. Seuferling, G. Münster, Nucl. Phys. B331 (1990) 515.
- [17] A. Hasenfratz, K. Jansen, Y. Shen, AZPH-TH 92-08, UCSD/PTH 92-08, BNL-47708.
- [18] W. Bock, C. Frick, J. Smit, J.C. Vink, Amsterdam preprint, ITFA-92-23 (1992).

## Figure captions

**Fig. 1.** The data for the upper and lower bounds on  $g_R$  as a function of  $G_{R\psi}^2$  together with the perturbative estimates for scale ratios  $\Lambda/m_{R\sigma} = 3$  (solid curve) and  $\Lambda/m_{R\sigma} = 4$  (dotted curve). Open points denote the data for the lower bound (points c, d, g in table 1), whereas full symbols are data for the upper bound. The  $6^3 \cdot 12$ -lattice is represented by triangles, whereas points on  $8^3 \cdot 16$  are denoted by squares.

**Fig. 2.** The mass ratio  $\mu_{R\psi}/m_{R\sigma}$  as a function of  $G_{R\psi}$  in comparison with one-loop perturbative estimates for  $m_{R\sigma} = 0.75$  (dotted curve),  $m_{R\sigma} = 1$  (full curve) and  $m_{R\sigma} = 1.25$  (dashed curve). The solid horizontal line represents the fixed point at infinite cut-off. The explanation of symbols is as in Fig. 1.

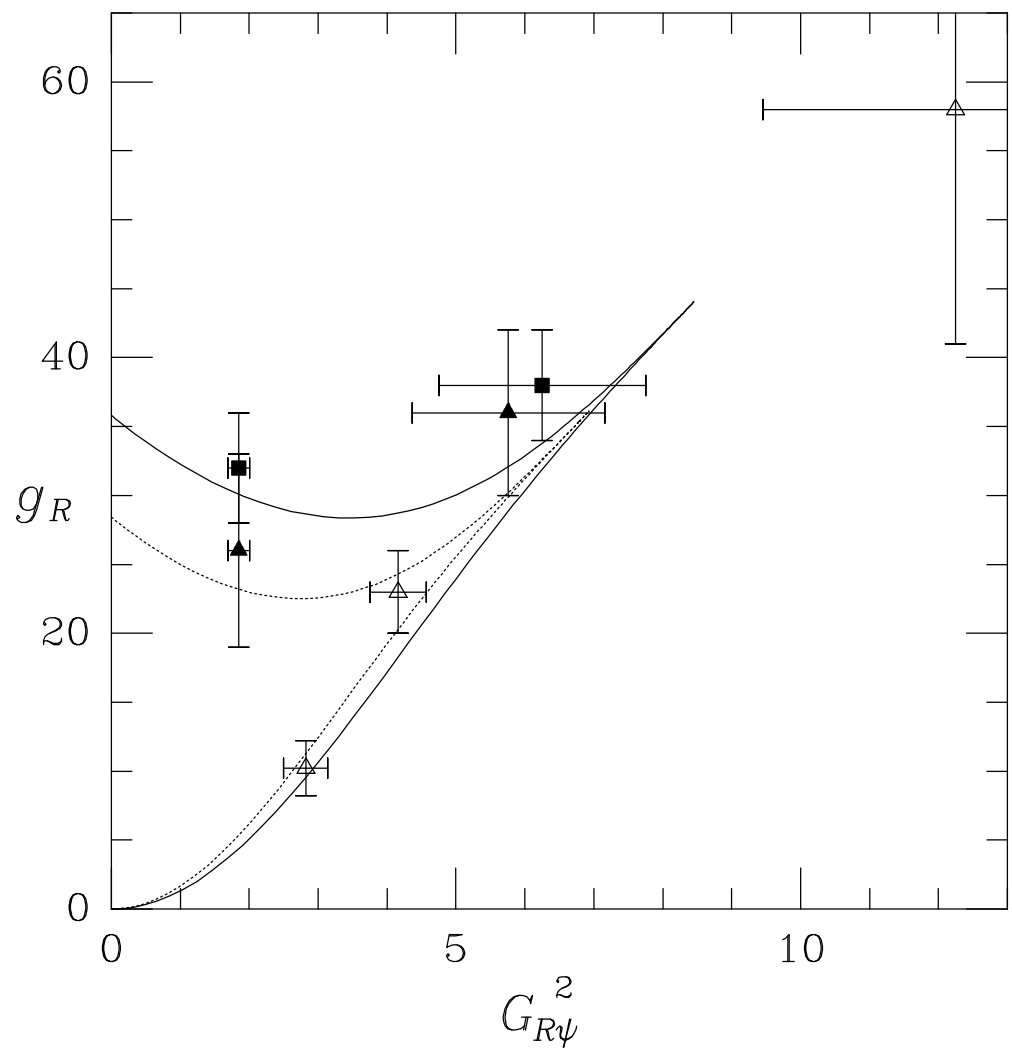


Figure 1

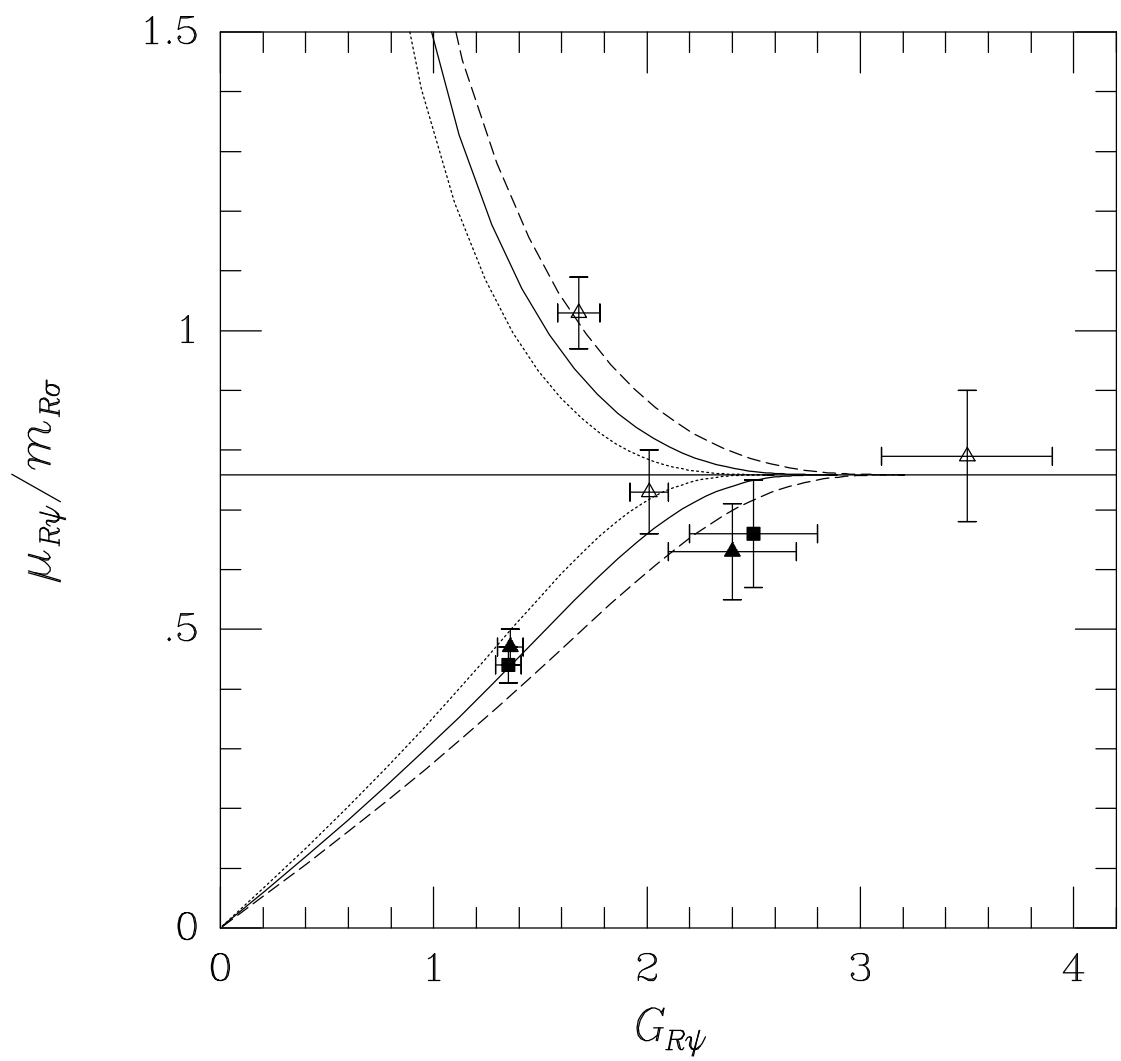


Figure 2